

Report on simulations and experiments on extraction and beam transport

Simulations

Various different attempts for the simulation of ion beam extraction and ion beam transport were made from the participating partners.

1. Ion beam extraction and ion beam transport (ATOMKI, GSI)

KOBRA3-INP has been used for the calculation of the electrostatic potential distribution, determined by the geometry. Different magnetic flux density distributions for different coil currents have been calculated with TOSCA and transferred to KOBRA3-INP. The wide range of possible magnetic settings of the ion source (which is set to a compromise between favorable extraction conditions and good confinement conditions for the plasma) increases the uncertainties for the simulation. Because both, electrons and ions are magnetized within the plasma (Larmor radius is in the sub mm range for both species) their motion is mainly along magnetic field lines. The value of magnetic flux density at the initial point of the magnetic field line (the assumed starting point of an ion) is crucial for the magnetic momentum $\int \mathbf{B} \cdot d\mathbf{s}$, responsible for the twisted behavior of each ion. Furthermore Figure 1 demonstrates that the initial location of the magnetic field line inside the plasma also depends on the azimuthal position.

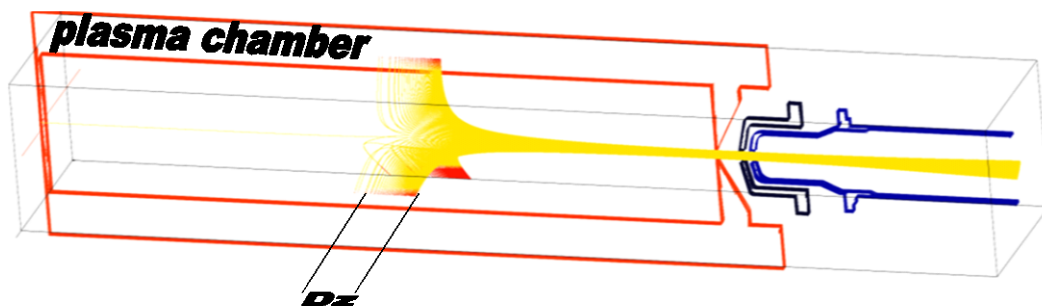


Figure 1: Magnetic field lines going through the extraction system (aperture radius = 5mm). Because of different starting points of the magnetic field lines, different $\int \mathbf{B} \cdot d\mathbf{s}$ will influence each trajectory. The three locations in the range Dz from where the ions are originating are shown. Regions with an initial flux density higher than in the extraction aperture are shown in red.

Because of the strong magnetic field collisions do not influence the path of the ions. If this would not be true, neither the observed structures of the extracted ion beam, nor the plasma traces on the plasma chamber could be explained. The general equations for modeling, especially the determination of electron density within the plasma, or quantities like plasma frequency, collision rate, and similar which are isotropic in the non-magnetic case here depend on the direction of the magnetic field. The exchange of momentum from the direction

of the magnetic field line into the plane transverse to it, depending on the gradient \mathbf{B} along the field line is taken into account. Furthermore, we assume that there is no $\mathbf{E} \times \mathbf{B}$ drift within the plasma because \mathbf{E} is small and hence negligible. It is assumed that the maximum available ion current density on each magnetic field line depends on the local electron density on each magnetic field line. As a conclusion the law of Child-Langmuir is still valid, but only locally for each magnetic field line.

To simulate that, the TrapCAD code developed by the ATOMKI ECR group has been used. It serves to simulate the spatial and energy structure of the lost and non-lost (i.e. plasma) electrons in ECR ion source plasmas. The spatial position and the energy evolution of a large number of electrons can be followed. By performing energy filtering on the plasma electrons one can draw conclusions even on the spatial positions of the highly charged ions in the plasma. As a result of the simulation non-lost electrons were studied which remain inside the plasma chamber. In Figure 2 the spatial distribution of the warm electrons (3-10 keV) are drawn in full and then only in the extraction side of the plasma chamber ($Z=130-220$ mm). This double filtering has been served as starting data for extraction simulation codes, where individual ions were started from the appropriate x-y-z coordinates where the ion density (i.e. warm electron density) is the highest.

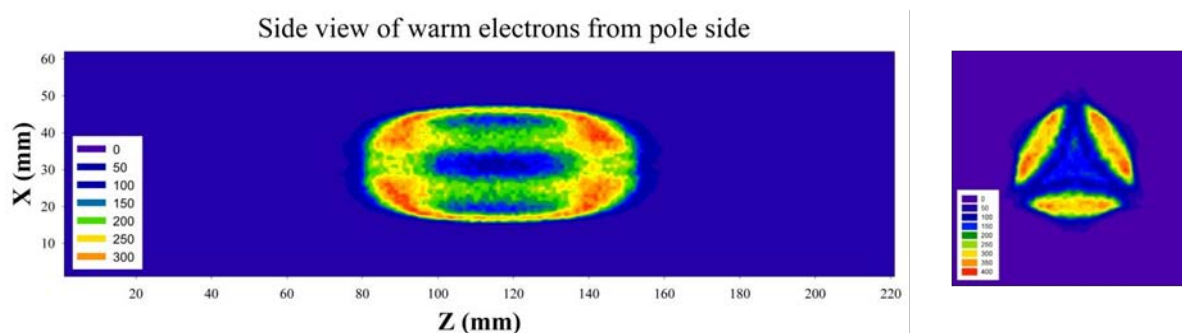


Figure 2: Side view of the warm electrons of the plasma (left) and axial projection of the warm electrons in the extraction side of the plasma chamber (right)

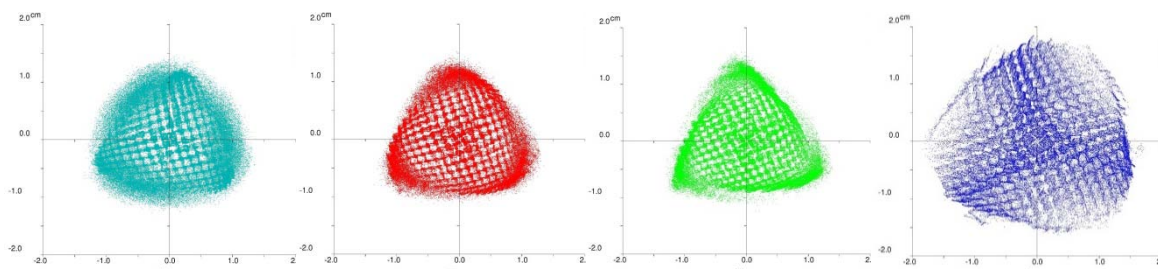


Figure 3: Ion beam profile of the extracted ion beam from left to right: Ar^+ , Ar^{3+} , Ar^{5+} , p . Whereas the proton fraction is already over focused by the solenoidal stray field, the Argon charge states show the typical three arm structure (simulated by KOBRA3-INP).

The ion beam structure observed in experiment could be reproduced with such a model (see Figure 3), which is not yet a validation of the assumed model, but a reasonable indication. The emittance is a useful quality measure for an ion beam; however, a simple projection of the 6D phase space in a 2D plotting area is not sufficient to describe the complicated structure. Attempts were made to overcome this problem. Instead of using the definition

$\mathcal{E}_{hor} = \iint f(x, y, x', y') dy dy'$ the integration should be avoided to obtain more information. Here f denotes the ion density distribution. Even coupling effects $\mathcal{E}_{x \rightarrow y}(x, y')$ can be investigated with such a measurement. We started to investigate different display options of the 4D (or even the 6D) phase space.

2. Ion beam extraction and ion beam transport (KVI)

At KVI simulations have been performed considering a He^+ beam extracted from the KVI-ECR ion source and transported to the image plane of the 110° analyzing magnet. The simulations have been checked by comparing them with both beam profile and emittance measurements. The objective of this work is a better understanding and improvement of the low-energy beam transport between the KVI-AECR ion source and AGOR cyclotron. The calculations consist of two parts, i.e. first we simulate the ion beam formation in the ECR plasma using a home-built PIC-MCC code which provides the phase-space coordinates of the He^+ ions in the plane of the plasma electrode. In a second step these coordinates are used as initial coordinates in ion trajectory calculations using the GPT code taking into account both space-charge forces and full three-dimensional maps of the external electric and magnetic fields in the simulation domain.

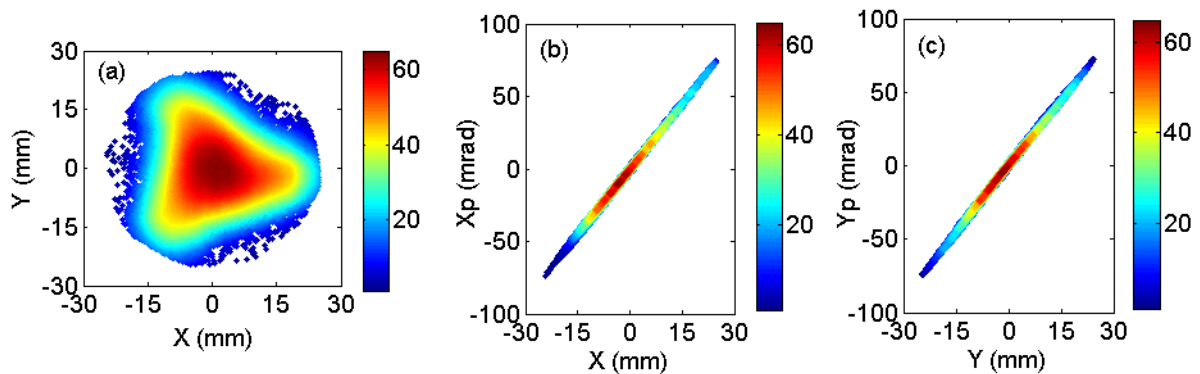


Figure 4: a) Calculated spatial distribution for a fully space-charge compensated 24 keV He^+ beam behind the ground electrode of the extraction system. b) Calculated horizontal and c) vertical emittance distribution of this beam at the same location.

The calculated spatial profile, horizontal emittance, and vertical emittance distributions of a 24 keV He^+ beam behind the ground electrode of the extraction system is shown in Figure 4 assuming full space-charge compensation. Figure 5 shows the corresponding results behind the analyzing magnet. Calculations with varying degrees of space-charge compensation were also performed showing that the effective beam emittance at this location strongly increases with decreasing space-charge compensation.

These beam simulations have been benchmarked by comparing them with beam profile measurements both behind the ground electrode and the analyzing magnet and with beam emittance measurements behind the analyzing magnet. The beam profile measurements have been done using a BaF_3 viewing target and CCD camera. These measurements only give qualitative information about the beam intensity because of saturation of the light yield with increasing current density. Comparison of the measured and calculated beam profiles shows good agreement and clearly favors full space-charge compensation. The emittance distributions behind the analyzing magnet have been measured with a pepper pot emittance

meter and are shown in Figure 9. The measured and the calculated emittance distributions show good agreement both qualitatively and quantitatively. The measured effective beam emittance in the horizontal plane is $390 \pi \text{ mm mrad}$ and in the vertical plane $320 \pi \text{ mm mrad}$, again clearly indicating full space-charge compensation.

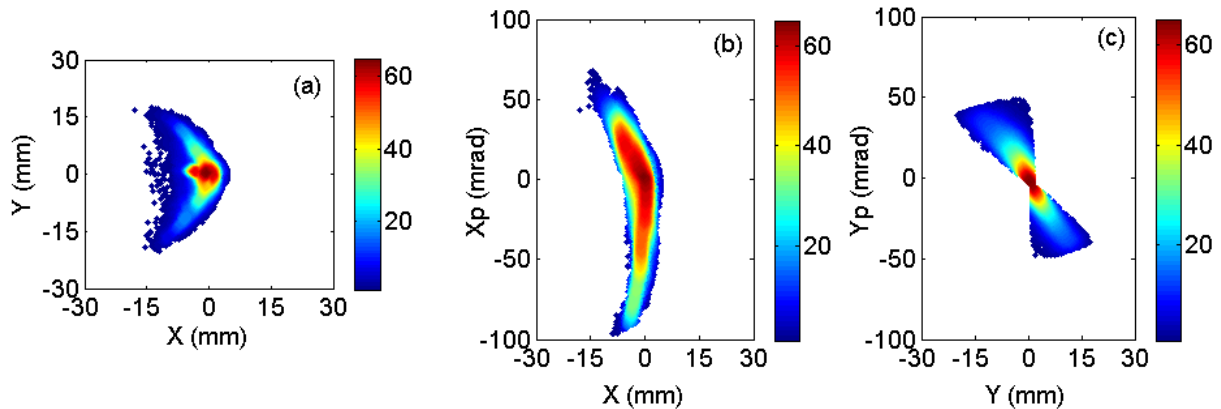


Figure 5: *a) Calculated spatial distribution for a fully space-charge compensated 24 keV He⁺ beam in the image plane of the analyzing magnet. b) Calculated horizontal and c) vertical emittance distribution of this beam at the same location.*

Beam losses which we also see in experiment are caused by the small vertical aperture of the analyzing magnet and its large second-order aberrations, which lead to an approximately six-fold increase of the effective beam emittance. Our simulations indicate that it is possible to partly compensate the second-order aberrations of the analyzing magnet by suitably shaping its pole faces. This will approximately double the beam transport efficiency.

Experiments

3. Ion source extraction and beam transport (JYFL)

A new extraction system has been designed and constructed for the JYFL 14 GHz ECRIS. The goal of the new design is to improve the performance of the ion source and increase the transmission efficiency of the low energy beam transport and the accelerator. The new extraction system is designed to be able to handle higher beam currents, yield better beam quality and offer more tuning flexibility. The design was made with the aid of simulations performed with the IBSimu code. The suitability of the code for this task was verified by simulating the old extraction system and good agreement between simulations and measurements was achieved. Figure 6 shows the comparison between the old and new extraction geometry when the total argon beam intensity of 1 mA is used in the simulations. The first experiments showed that the beam intensities after the K130 cyclotron increased even by a factor of 2. A series of transmission measurements has been performed with $^{40}\text{Ar}^{8+}$ ion beams to compare experimentally the performance of the old and the new extraction systems. As a result the respective transmission increased from about 2.3% to 4.6%.

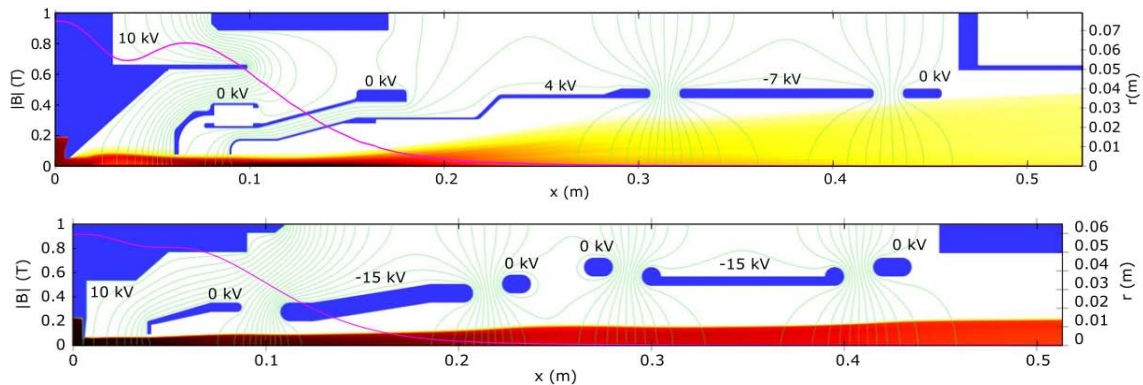


Figure 6: Simulation result (trajectory density) of the old (upper picture) and new extraction system (lower picture). Voltage of each electrode is shown and the solid purple line indicates the magnetic field on axis.

In 2009 it was presented [V. Mironov et al., presentation at the 37th European Cyclotron Progress Meeting, October 28–31, 2009, Groningen, Netherlands and personal communication (2009)], that using a so-called collar structure around the extraction aperture could yield improved ECR ion source performance by shifting the charge state distribution of ions towards higher values. A detailed study using this structure was performed at the JYFL 14 GHz ECRIS by varying the length and material of the collar (see Figure 7).

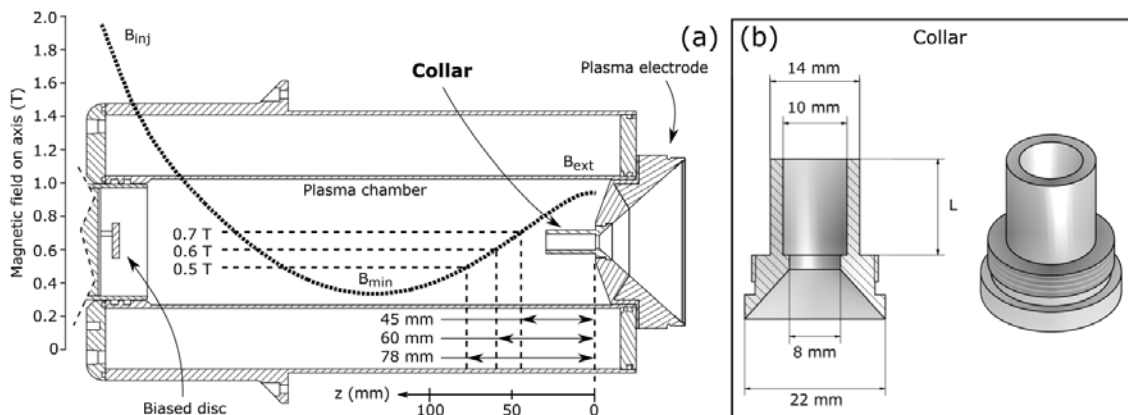


Figure 7: A schematic presentation of the collar installed to the plasma electrode of the JYFL 14 GHz ECRIS (a) and the structure of a separate collar (b). The solenoidal magnetic field on axis is also presented with $B_{inj} = 1.95$ T, $B_{min} = 0.35$ T and $B_{ext} = 0.94$ T. The collar length L , defined in part (b) of the Figure, was varied between 0 and 60 mm. In the Figure $L = 30$ mm in the schematic plasma chamber assembly (a) and $L = 15$ mm for the presented separate collar (b).

The experiments show that surprisingly long (up to 30 mm) collar structures can be implemented without degrading the ion source performance in terms of extracted beam current and transverse emittance. For some beams a moderate performance improvement was obtained with the collar. It is concluded that based on the results obtained with the JYFL 14 GHz ECRIS, the collar structure itself does not provide remarkable improvement to ECRIS performance. However, there may be room available for technological improvements around the extraction region.

4. Ion beam transport (GSI)

The CAPRICE-type ECRIS at the ECR injector test setup (EIS) has been operated with a Travelling Wave Tube Amplifier (TWTA). Frequency sweeps in the range 12.5-16.5 GHz were performed at a microwave power of 450 W injected into an Ar/He plasma optimized for the production of an Ar¹¹⁺ ion beam. Some frequencies can be identified at which the Ar⁹⁺ ion currents ($q = 8, 9, 11, 12$) are considerably enhanced with respect to the standard operating frequency of 14.5 GHz. For the prominent frequency of 13.221 GHz a comparison of the beam transmission was performed with respect to the operating frequency of 14.5 GHz both as a function of microwave power varying over a wide range from 250 W to 550 W. The transmitted ion beam current includes the sum of all m/q -ratios from 1 to 20 and was correlated with the total current of ion source extraction. As Figure 8 shows a clear enhancement of the transmission is achieved when the microwave frequency is set to an optimized condition.

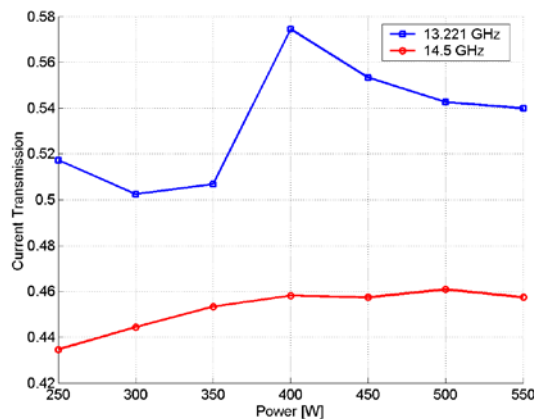


Figure 8: Transmission of an Ar/He ion beam through the LEBT for different microwave frequencies (all other ion source parameters were kept constant).

5. Ion beam transport (KVI)

The transport of a heavy-ion beam extracted from an Electron Cyclotron Resonance Ion Source (ECRIS) often shows significant beam losses. For example, at KVI the 25 m long beam line between the ECRIS and the AGOR cyclotron has a typical transmission of 16%. The cause of this low transmission has been mainly attributed to emittance blowup in the 110° (double focusing) analyzing magnet caused by its second-order aberrations in combination with the relatively large divergence of the extracted ion beam. This is illustrated in Figure 9 which shows the measured phase-space distributions of a 24 keV He⁺ beam close to the image plane of the analyzing magnet. While the He⁺ beam has an emittance of 65 mm-mrad (both horizontally and vertically) in the object plane before the magnet, the measured emittances behind the magnet are 390 mm-mrad horizontally and 320 mm-mrad vertically. The simulations have been performed as described in Chapter 2 assuming a fully space-charge compensated beam. As can be seen, there is good agreement between the simulated and measured phase-space distributions.

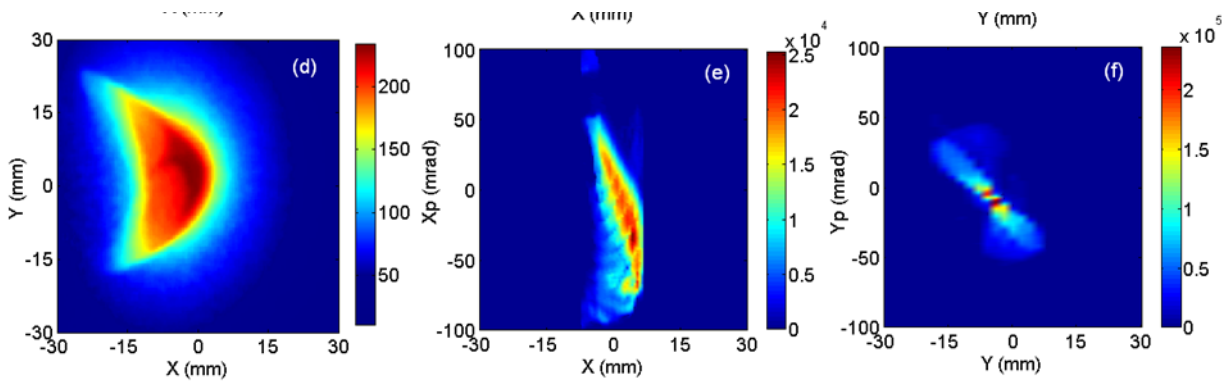


Figure 9: Measured spatial and transverse phase-space distributions of a 24 keV He^+ beam close to the image plane of the 110° analyzing magnet. Compare with the simulated phase space distribution in Fig.5.

It has been shown that the emittance blowup in the analyzing magnet can be largely prevented by i) increasing the magnet gap from 67 to 110 mm and by ii) suitably modifying the pole surfaces of the analyzing magnet in order to compensate its second-order aberrations. This can be done by giving the entrance and exit sections of the pole surfaces a concave shape and the central part a convex shape. Simulations show that such a modified analyzing magnet will have horizontal and vertical emittances in the image plane of 230 and 100 mm-mrad, respectively, which is a significant improvement compared to the uncorrected magnet. However, compensating the second-order aberrations of the analyzing magnet in this way is rather expensive and a similar reduction of the beam emittance can be realized by placing an electrostatic Einzel lens between ion source and analyzing magnet. Using COSY INFINITY we have calculated a 5th-order transfer map which maps the transverse phase-space coordinates of a He^+ ion at a longitudinal position of 710 mm before the analyzing magnet to the image plane 544 mm behind the analyzing magnet.

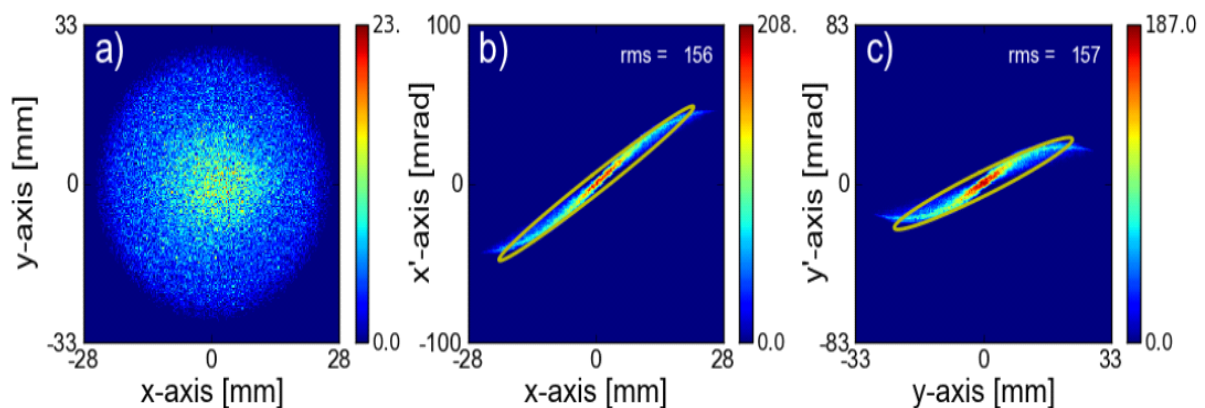


Figure 10: Calculated spatial and transverse phase-space distributions of a 24 keV He^+ beam in the image plane of the analyzing magnet. (a) spatial distribution, (b) horizontal phase-space distribution, (c) vertical phase-space distribution.

6. Space charge compensation (JYFL)

Space charge compensation was investigated in front of and behind the analyzing magnet. A positively biased grid was installed and tested in the beam line. The experiment showed that even a small disturbance in the density of compensating electrons between the ion source and the analyzing magnet results in severe deterioration of the beam properties. The removal of electrons has clear degrading effect on the beam quality. Increasing the number of electrons via neutral gas injection and subsequent ionization by the ion beam clearly improves the beam quality. This underlines the important role of space charge compensation in achieving good beam quality. Downstream from the analyzing magnet the effect was negligible indicating that the space charge related problems are very localized to the region of high beam current. The beam divergence of the JYFL 14 GHz ECRIS was also studied in order to perform more accurate and realistic beam optical simulations, which are required for the upgrade of high intensity section of the low energy beam line. According to the experiments the divergence is 30 – 70 mrad and depends strongly on the operation conditions of the ECRIS.

7. Space charge compensation (GSI)

The degree of space charge compensation is determined by the total amount of generation and losses of compensating particles which may be created by collisions of primary fast ions with residual gas atoms or with solid surfaces.

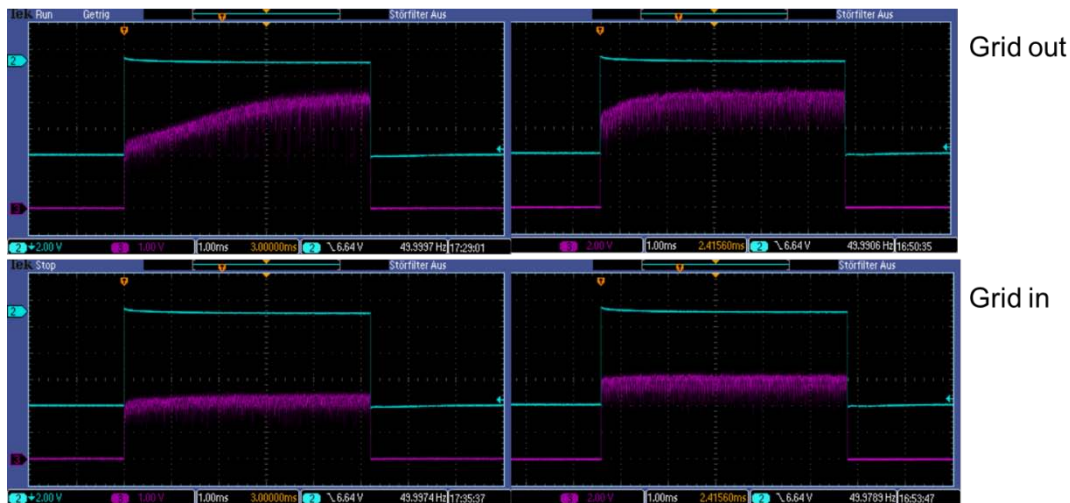


Figure 11: Faraday cup signals from singly charged Helium beam (violet). Left: energy 5keV, current 400(200) μ A, right: energy 10keV, current 800(600) μ A. Intensity in bracket denotes the intensity, when the grid is inserted into the beam line. The chopper timing gate pulse is shown in blue. Space charge compensation time: left $\tau=3.5$ ms, right $\tau=1$ ms. The pressure in that part of the beam line was in the range of 10^{-7} mbar.

To investigate the behavior of space charge compensation an electrostatic chopper was used consisting of two parallel plates. The chopper is installed directly behind the analyzing dipole magnet of the low energy beam transport which is equipped with a CAPRICE-type ECRIS. The chopper plates are switched from 0 V to voltages of about +4 kV and -4 kV, respectively. Thus the chopper deflects the analyzed beam from the beam line axis in vertical direction within 1 μ s. This time is much smaller than the necessary time to build up the space charge

compensation. As soon as the chopper is grounded to 0 V again, the beam will pass the chopper on axis, and the build-up of space charge compensation can start. When the intensity becomes constant, the divergence of the ion beam does not change any more and it is assumed that the ion beam is space charge compensated after that time. Instead of varying the pressure to reduce the space charge compensation time, the wires of a grid profile monitor were utilized to provide a sufficient number of secondary electrons for compensation (see Figure 11). However, it has to be pointed out, that the degree of space charge compensation varies along the beam line, because the beam plasma conditions are different along the beam line. In regions, where the magnetic flux density is negligible, the beam plasma will behave as electric plasma, whereas in regions with magnetic flux density, the electrons become magnetized. Assuming that the production rate of electrons is larger than the loss rate of compensating electrons, it is only a question of time until space charge compensation is completed. The ion beam transport from the source to the chopper is made with full space charge compensation, because all necessary precautions are taken to keep the space charge compensation effective.

8. Ion beam properties (JYFL)

A versatile measurement system is composed of data acquisition hardware and software for measurement and analysis. The measurements with the JYFL 14 GHz ECRIS showed that the ion beams exhibit periodic current fluctuations at frequencies from 100 Hz to 1.5 kHz with amplitudes ranging from 1 to 65 percent of the average beam current.

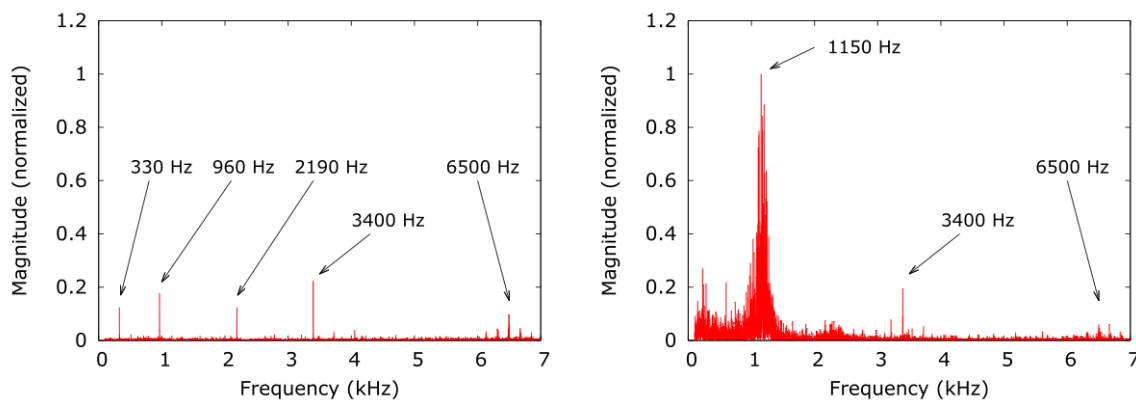


Figure 12: Left: typical background frequency spectrum measured from the first Faraday cup after m/q separation (FC2). Right: the frequency spectrum with $110 \mu\text{A } ^{40}\text{Ar}^{8+}$ beam. The spectra are shown up to the RC circuit cutoff of the measurement system (7 kHz).

Figure 12 shows a comparison of typical frequency power spectra measured from the Faraday cup without the ion beam (background) and with $110 \mu\text{A } ^{40}\text{Ar}^{8+}$ beam. The influence of the beam on the spectrum is concentrated to frequencies of ~ 1 kHz and dominates over the background. It was observed that the beam current oscillation characteristics vary slightly with time. To better characterize the oscillations, each of the studied cases (ion source tunes, etc.) was measured up to 20 times in sequence. Variation of the ion source settings (in this case the microwave power) alters the beam current oscillation behavior of $^{16}\text{O}^{6+}$ beam dramatically. Similar beam characteristic and instability behavior was measured from different Faraday cups along the beam line.

9. Ion beam properties (GSI)

Ion beams extracted from an ECRIS are in most cases characterized by an internal structure with inhomogeneous current density distribution. Viewing targets (VT) can be used to obtain a qualitative 2D image of the beam profile. For quantitative measurement of spatially resolved 2D current density distributions a multiple Faraday cup array (FCA) is a versatile tool. An in-situ comparison of VT and FCA performed at GSI in cooperation with L. Panitzsch (Institute for Experimental and Applied Physics, University of Kiel, Germany) could confirm good agreement (see Figure 13).

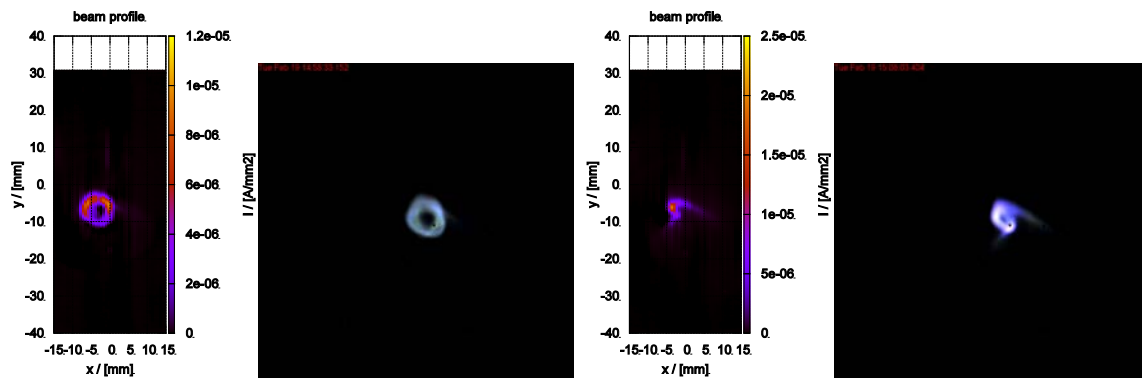


Figure 13: Comparison of identical ion beams quasi-simultaneously measured with FCA and viewing target VT for two different solenoid settings.

10. Emittance measurements and pepper pot emittance meters (GSI, KVI)

Typically, the beam quality is described by its emittance, which is mostly defined for both transversal planes x , and y :

$$\varepsilon_x = \iint f(x, x') dy dy', \text{ respectively } \varepsilon_y = \iint f(y, y') dx dx'$$

However, this assumes the permissibility to separate both transverse coordinates x and y , which is not the case because of the magnetic field. As a consequence, a usual device to measure the ion beam emittance, like an Allison scanner, is not useful. A pepper pot emittance measuring device provides more detailed information about the beam quality. This was the starting point for the development of emittance meters dedicated to perform measurements at the the EIS test bench at GSI. The design and construction was performed at KVI. After this pepper pot emittance meter had been commissioned and applied for first experiments at KVI it was implemented and commissioned at the EIS test bench of GSI and was prepared for experiments to be compared with those mentioned above. The analysis of such pepper pot data is a sophisticated problem due to its 4D-characteristics. Experimental difficulties have to be solved like the unambiguous assignment of the image spot to the origin of the corresponding beam sector. Furthermore it is evident, that the data presentation used for the projection of the 4D phase space into the 2D plotting area cannot be used to image the 4D information $\varepsilon(x, y, x', y')$. Because of the limitation in presentation, a series of graphics $\varepsilon_y(x, x', y')$, $y=y_1 \dots y_n$ is proposed.